Scripta Materialia 194 (2021) 113680

Contents lists available at ScienceDirect

Scripta Materialia

journal homepage: www.elsevier.com/locate/scriptamat

Surfactant effect of impurity sulphur in ductility dip cracking of a high-chromium nickel model alloy

A. Rapetti[a,b], F. Christien[c,*], F. Tancret[b], P. Todeschini[a], S. Hendili[d], J. Stodolna[a]

[a] EDF R&D, Materials and Mechanics of Components Department, F-77818 Moret-sur-Loing, France
[b] Université de Nantes, Institut des Matériaux Jean Rouxel (IMN), Polytech Nantes, BP 50609, 44306 Nantes Cedex 3, France
[c] Mines Saint-Etienne, Univ Lyon, CNRS, UMR 5307 LGF, Centre SMS, F - 42023 Saint-Etienne, France
[d] EDF R&D, Industrial Risk Management Department, F-78400 Chatou, France

ARTICLE INFO

Article history:
Received 24 September 2020
Revised 19 November 2020
Accepted 16 December 2020
Available online 29 December 2020

Keywords:
Interface segregation
Grain boundary embrittlement
impurity embrittlement
Welding
Ductility dip cracking

ABSTRACT

The sensitivity to ductility dip cracking was measured in two model high chromium nickel alloys, with the same composition, apart from different sulphur contents. The newly developed Refusion Cracking Test was used, that consists in repetitive refusion lines conducted at the specimen surface. Grain boundary cracks develop in the heat affected zone near the refusion line. Cracking is much more pronounced in the sulphur-enriched alloy, which demonstrates a strong deleterious effect of sulphur. However post-mortem analyses using WDS and STEM-EDS revealed no segregation of sulphur at grain boundaries. In contrast, grain boundary fracture surfaces are covered with sulphur. This suggests a dynamic type of grain boundary embrittlement where sulphur acts as a surfactant, facilitating crack opening. Sulphur is efficiently provided to the crack tip as it propagates, due to accelerated diffusion by plastic deformation. This allows crack growth rates higher than 10 µm/s.

Austenitic materials are prone to "ductility trough" at temperatures between 0.5 and $0.8T_M$ (melting temperature), which manifests itself in grain boundary (GB) cracking and limited elongation to fracture. This phenomenon is also termed "intermediate temperature embrittlement", "hot-shortness" or "ductility dip cracking" (DDC). The detrimental effect of trace elements, especially sulphur, in DDC of steels [1,2], nickel [3–5] and copper [6] alloys was demonstrated in early works, using model alloys of well controlled composition at the ppm level, so as to unambiguously identify the impact of particular trace elements. However, some examinations conducted in more recent studies [7,8] of DDC cracked specimens of different materials using advanced characterisation techniques, like Transmission Electron Microscopy or Atom Probe Tomography, failed in demonstrating the segregation of sulphur at GBs. In view of those studies, the role of sulphur in DDC can indeed be questioned.

High chromium nickel alloys are widely used in the primary circuit of pressurized water nuclear reactors. Numerous studies have shown that those alloys can be sensitive to DDC, especially in welding conditions (see for example the background section in [9]). In the present work, DDC is studied on model alloys of identical composition with controlled additions of sulphur in order to unambiguously demonstrate the potentially detrimental effect of this element. Complementary chemical analyses of uncracked and cracked grain boundaries are conducted to investigate the influence of sulphur on embrittlement mechanisms. The sensitivity to DDC is determined using the newly developed RCT test (Refusion Cracking Test) [9,10], that is well adapted to the study of model alloys, where only limited amounts of materials are available. Post-mortem chemical analyses of GBs were conducted in order to question the occurrence of sulphur GB segregation. A control specimen with a known amount of sulphur GB segregation was used to validate the characterization methodologies. The GB cracking mechanism is discussed in the frame of a dynamic type of GB embrittlement due to sulphur.

The materials used in this study are two model alloys of controlled purity with similar composition as 690 alloy (Table 1). 0.5 kg of each alloy was obtained using vacuum melting in a cold silver crucible. After solidification, the ingots (25 × 25 × 100 mm) were transformed into plates (7 × 50 × 170 mm) by hammering at room temperature. The first alloy (Base) displays a very low sulphur content whereas the second alloy (Base+S) is enriched in sulphur. Apart from sulphur, the composition of the two alloys is the same. In addition, pure nickel containing 5.4 wt ppm of sulphur was used as a control specimen for sulphur segregation measurements.

* Corresponding author.
E-mail address: frederic.christien@emse.fr (F. Christien).

https://doi.org/10.1016/j.scriptamat.2020.113680
1359-6462/

Table 1
Composition of the model alloys used in this study.

	Ni	Cr	Fe	Mn	Si	Ti	Al	C	N	O	S
Alloy	Wt %							Wt ppm			
Base	*	29.9	8.42	0.85	0.14	0.21	0.13	11	1	7	**4.7**
Base+S	*	30.0	8.44	0.84	0.14	0.21	0.13	16	1	7	**52**

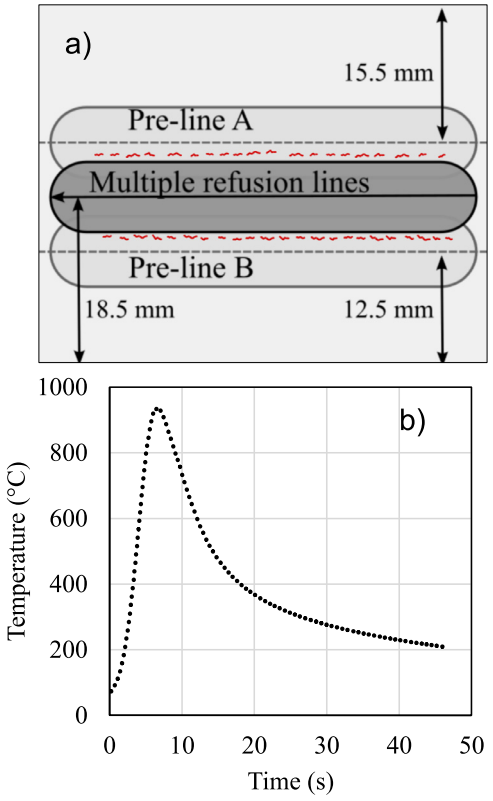

Fig. 1. a) Principle of Refusion Cracking Test. Small red lines represent cracks. The length and width of pre-lines and refusion lines are 45 mm and 8 mm respectively. b) Typical temperature cycle measured during a RCT pass using a thermocouple located in the cracking region.

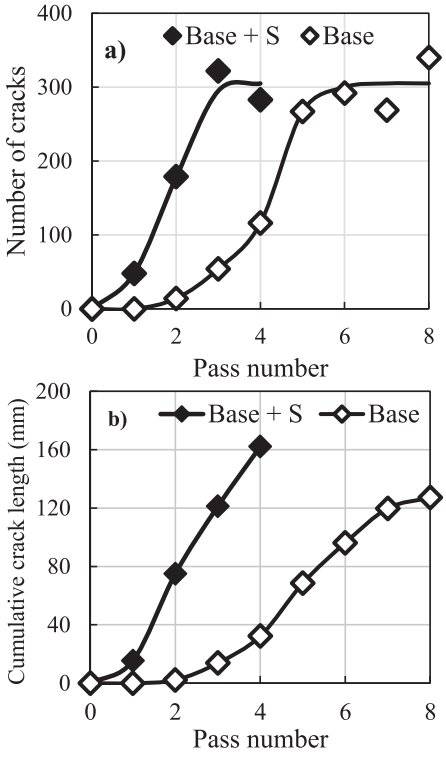

Fig. 2. RCT results for Base and Base+S alloys. a) Number of cracks. b) Cumulative crack length.

RCT was conducted in order to assess the sensitivity to DDC of the two alloys. It consists in multiple GTAW (Gas Tungsten Arc Welding) refusion passes performed between two initial pre-passes. The procedure is detailed in [9,10] and schematically reminded in Fig. 1a). The procedure ensures that the Heat Affected Zone (HAZ) of the central passes are located in the welding solidification microstructure, which makes the test representative of actual welding conditions prone to DDC [11]. The sample dimensions are 50 × 40 × 7 mm. A welding speed of 11 cm/minute, a voltage of 10V and an intensity of 120A were used. Eight and four refusion passes were carried out on the Base and Base+S alloys respectively. After each pass, a binocular magnifier was used to measure the number of cracks and the cumulative crack length at the specimen surface. Cracks are located at distances ranging approximately from 0.4 to 2.2 mm from the melt pool, i.e. in the HAZ. Fig. 1b) shows the typical temperature cycle measured during a pass using a thermocouple located at the centre of the cracking region. Thermomechanical simulation of the RCT test was conducted in [12] on a 52M Inconel alloy, having a composition very close to that of the materials studied here. The simulation showed that the maximum tensile stress that develops in the HAZ perpendicularly to the welding direction during a pass is about 300 MPa. In addition, the cumulated plastic deformation is as high as 25% in the HAZ after five passes.

Sulphur GB segregation was measured using WDS (Wavelength Dispersive X-ray Spectroscopy) in the SEM (Scanning Electron Microscope) according to the methodology developed by Christien and Risch [13]. This methodology consists in acquiring concentration line scans of the segregated solute across the boundary. The apparent concentration peak obtained is a convolution of the actual concentration profile (here extremely narrow, i.e. ~ 1 nm) with the probe function (~ 1 μm). Quantification of the segregated element is obtained from integration of the concentration peak area and is expressed as a mass of sulphur per unit GB area (nanograms/cm^2). More details about the methodology and the system used can be found in [13]. Additional sulphur segregation observations were conducted using EDS (Energy-Dispersive X-ray Spectroscopy) on FIB (Focused Ion Beam) lamellas in a FEI Osiris S/TEM (Scanning Transmission Electron Microscope) equipped with the SuperX system consisting of four EDS spectrometers. The lamellas were prepared in a FEI Helios Nanolab. The final ion thinning was obtained in a PIPS II system from Gatan at 500 V. Lamella thicknesses below 70 nm were obtained. The STEM beam voltage and current were 200 kV and 2 nA respectively and the probe size was approximately 0.5 nm. Sulphur mapping was conducted in the scanning mode at a resolution of ~500 × 1000 pixels and the exposure time per pixel was 10 ms.

Fig. 2 presents the results obtained for the two alloys tested using RCT, i.e. the number of cracks and the cumulative crack length as a function of the number of passes. A strong detrimental impact of sulphur on the resistance to DDC is observed. The Base+S alloy

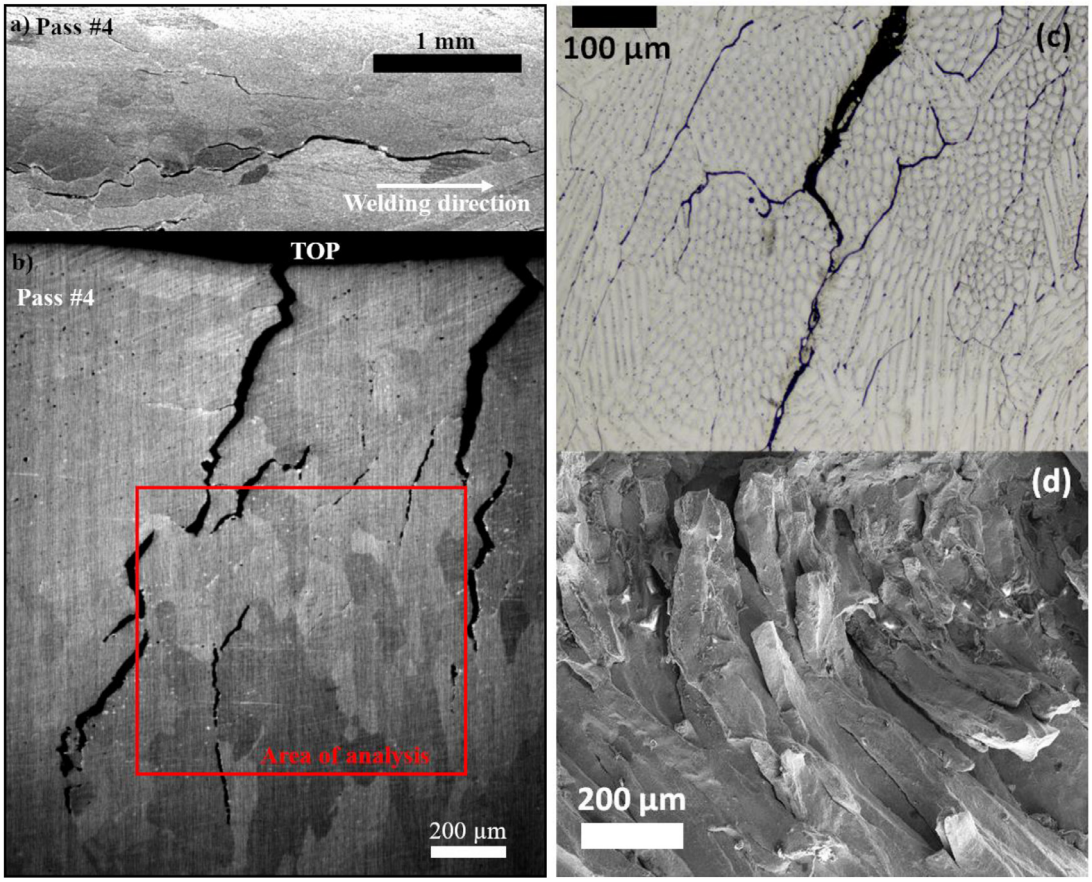

Fig. 3. Observations of Base+S sample after four RCT passes. a) SEM surface observation, b) SEM cross-section observation, c) optical cross-section observation, d) SEM observation of the fracture surface of a crack.

shows numerous cracks after only one pass, in contrast to the Base alloy. After two passes, both alloys show cracks, but the cumulative crack length is higher by a factor of 35 in the Base+S compared to the Base alloy. The number of cracks saturates at about 300 for the two alloys.

Fig. 3 (a) presents a SEM surface observation of the Base+S sample after four RCT passes. Intergranular cracks are clearly visible. It was shown in a previous study that those intergranular cracks are entirely located in the HAZ and are the result of DDC, not liquid cracking [9]. Fig. 3 (b) is a SEM cross-section view of the cracking area. The optical micrograph in Fig. 3 (c) also revealed the dendritic solidification microstructure, with a dendrite arm size of approximately 10 to 20 µm. It is observed in Fig. 3 (c) that most of the grain boundaries do not coincide with interdendritic spaces, which means that they have migrated after solidification, so that their embrittlement is independent of interdendritic solidification microsegregation. Fig. 3 (d) shows the fracture surface of a crack. The intergranular nature of the fracture is confirmed. The red rectangle in Fig. 3 (b) indicates the area where GBs were selected for analysis.

WDS line scans were performed across eleven GBs in the cracked area (red rectangle in Fig. 3b)). Only uncracked GBs were selected for WDS analysis. As WDS is not among the common techniques to study monolayer segregation, a control specimen was used to ascertain the capability of the methodology to detect sulphur segregation in the submonolayer range. This control specimen is pure nickel containing 5.4 wt ppm of bulk sulphur. It was heat treated 100 days at 550°C to obtain a segregation level of some tens of ng/cm^2. Sulphur GB segregation in nickel was extensively studied in previous works using SIMS [14], Auger [15,16] and WDS [13,17,18]. Fig. 4a) presents examples of GB sulphur profiles obtained in the Base+S alloy (after four RCT passes) and in the control specimen. The sulphur segregation peak is clearly observed in the control specimen as expected. In contrast, no sulphur peak is obtained for the GB analysed in the Base+S alloy after four RCT passes.

Fig. 4b) presents the GB sulphur concentrations obtained using the quantitative methodology described in [13] for the control specimen and for the Base+S model alloy after four RCT passes. Sulphur is detected in all the GBs analysed in the control specimen. The average sulphur GB concentration is 54 ng/cm^2, i.e. ~10^{15} S atoms/cm^2 or 0.55 monolayer, considering that a "monolayer" is a (111) close-packed plane of nickel. In contrast no sulphur segregation is detected in any of the GBs analysed in the Base+S alloy after four RCT passes. This means that no sulphur segregation exists in that specimen or it is below the limit of detection (previous studies have shown that the limit of detection of the WDS methodology is of a few percents of a sulphur monolayer [13,18]).

STEM-EDS mapping of sulphur on FIB lamellas were performed on one GB of the control specimen and two GBs of the Base+S model alloy (Fig. 5), including a cracked GB. Sulphur segregation is observed for the control specimen (Fig. 5 a)), which also confirms the ability of the STEM-EDS methodology to detect solute GB segregation in the sub-monolayer range. In contrast, no sulphur segregation is found in the first GB of the Base+S RCT specimen (Fig. 5 b)), which agrees with the previous WDS results. However strong sulphur segregation is found in the cracked GB (Fig. 5c)). It can be observed that sulphur covers the two surfaces of the crack. The interior of the crack is found to be enriched in oxygen, which shows the formation of an oxide layer. This oxide layer is located on top

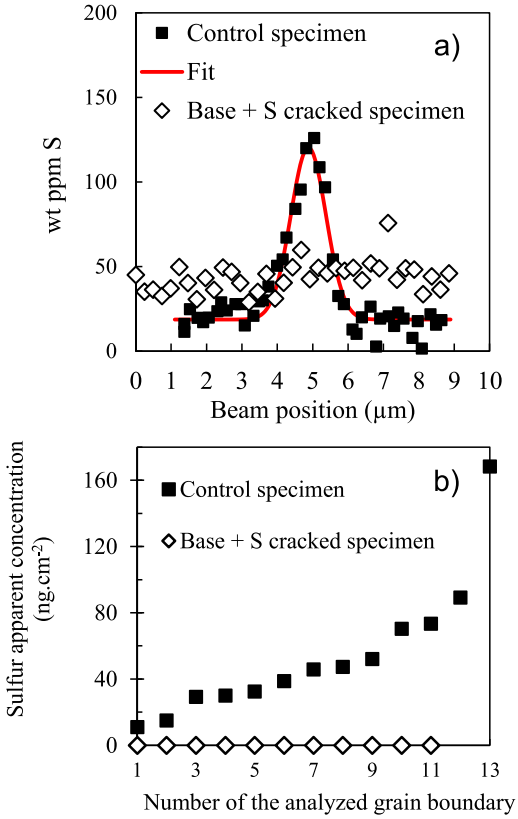

Fig. 4. a) Examples of GB sulphur line scans obtained using the WDS methodology in the Base+S specimen (after four RCT passes) and in the control specimen. b) Sulphur GB concentration estimated in thirteen GBs of the control specimen and eleven GBs of the Base+S RCT specimen.

of the sulphur segregation layer, which suggests that oxidation occurred after sulphur segregation.

RCT tests conducted on model alloys clearly demonstrated that the sulphur-enriched alloy is much more sensitive to cracking (Fig. 2). It should be noted that model alloys were used in this study, differing only in their sulphur content, so that there cannot be any ambiguity on the detrimental effect of this element. As the cracks obtained are all intergranular, it is quite natural to suspect that the metallurgical cause of cracking is the GB segregation of sulphur. However the numerous GB analyses (Figs. 4 and 5b)) conducted on the post-mortem RCT specimen have revealed no sulphur segregation at all in uncracked boundaries. Similar attempts to demonstrate the GB segregation of sulphur on DDC cracked specimens of nickel alloys were made in previous studies by Noecker et al. [7]. As no sulphur GB segregation was found, those authors concluded that sulphur was not involved in the mechanism of DDC. However their conclusion can be questioned in view of the results obtained in the present study: despite the absence of sulphur segregation in uncracked GBs, the detrimental effect of sulphur is not in doubt here, considering the results of Fig. 2.

In contrast to uncracked GBs, the STEM-EDS analysis conducted on a cracked GB has shown the strong segregation of sulphur at the cracked surfaces (Fig. 5c)). This suggests that the mechanism of cracking is of dynamic type, i.e. the cracked surfaces are gradually covered with sulphur at the same time as the crack propagates. Sulphur segregation to the surfaces of the opening crack results in a reduction of the surface energy, which facilitates crack opening, according to the Griffith criterion for example [19]. This mechanism was rationalised by the "slow fracture" approach [20,21] in which the chemical potential of the segregating solute is consid-

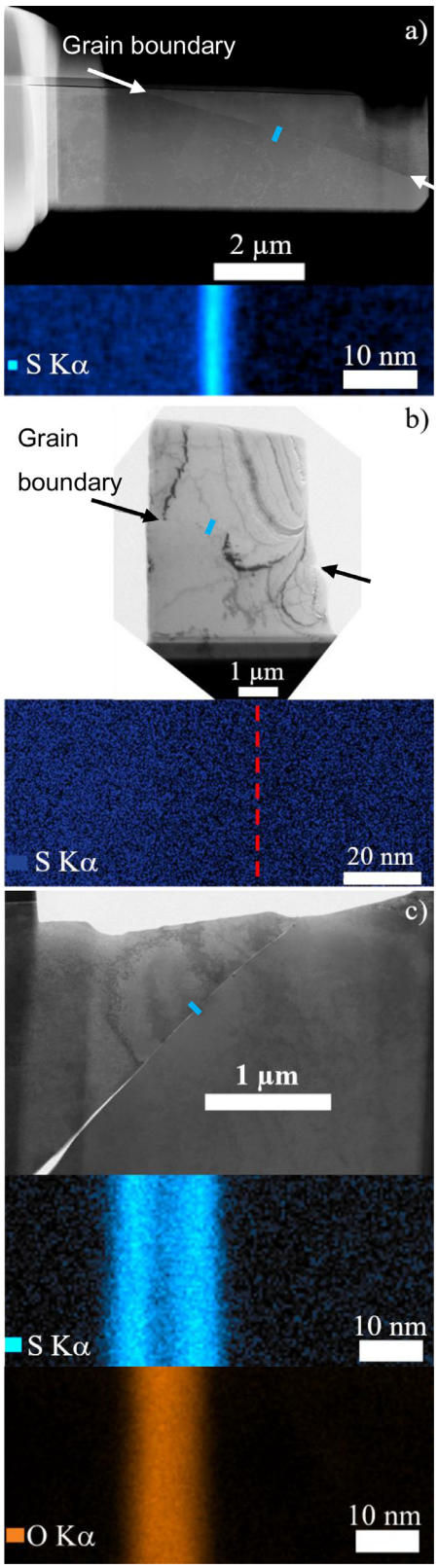

Fig. 5. STEM-EDS mapping on GBs. a) control specimen, b) uncracked GB and c) cracked GB in Base+S RCT specimen. The dashed red line indicates the GB location. Blue rectangles in images indicate the mapped areas. The images were obtained using STEM high-angle anunular dark field for a) and bright field TEM for b) and c).

ered constant as the GB opens. This implies a change in composition of the two surfaces created by the propagating crack. The sulphur acts here as a "surfactant" facilitating the creation of new surfaces [22]. Of course this scenario is possible only if the transport of sulphur is fast enough to "feed" the propagating crack tip. Kirchheim et al. [22] have proposed a criterion to assess the possibility of such a process. The crack growth rate da/dt (m/s) has to be below a certain value given by Eq. 1:

$$\frac{da}{dt} \leq \frac{2\pi DC_b}{\Gamma} \quad (1)$$

where D is the solute diffusion coefficient (m^2/s), C_b is the solute content in solid solution (m^{-3}), Γ is a threshold surface solute concentration (m^{-2}) needed to allow the dynamic opening of the grain boundary. Eq. 1 can be adapted to the non-isothermal conditions of the RCT tests conducted here:

$$a \leq \frac{2\pi C_b}{\Gamma} \int_0^{t_p} D(t)dt \quad (2)$$

a is the increase in crack length obtained in one RCT pass, t_p is the duration of the RCT pass. Considering the temperature cycle shown in Fig. 1b) (corresponding to the centre of the cracking region), the evolution with time of the diffusion coefficient $D(t)$ can be determined using $D = D_0 \exp(-Q/RT)$, $D_0 = 1.4$ cm^2/s and $Q = 218.6$ kJ/mol (bulk diffusion coefficient of sulphur in nickel [23]). With $C_b = 52$ wt ppm $= 8.3\ 10^{18}$ cm^{-3} (for the Base+S alloy) and $\Gamma = 1/3$ monolayer $= 6\ 10^{14}$ cm^{-2}, the estimated increase in crack length a for one RCT pass is about 1 µm. The value considered for Γ is somewhat arbitrary but this is not going to affect significantly the order of magnitude obtained for a.

On the other hand, the actual increase in crack length per pass can be roughly estimated from the RCT data shown in Fig. 2. For the Base+S alloy, the number of cracks (Fig. 2a)) does not change between passes 3 and 4. Consequently, the corresponding increase in cumulative crack length (Fig. 2b)) is due to propagation of existing cracks, not to the onset of new ones. The increase in crack length can then be simply estimated by dividing the increase in cumulative crack length (+ 40 mm) by the number of existing cracks (~300), which results in an individual increase in crack length of ~130 µm per RCT pass. This indicates that the cracks are actually propagating faster by two orders of magnitude than predicted by Eq. 2 (~1 µm). Assuming that the time allowed for crack propagation during one RCT pass is roughly about 10 s (i.e. the time spend above ~500°C in Fig. 1b)), the average crack growth rate is at least 13 µm/s. This is not unreasonable since previous works on sulphur-induced dynamic embrittlement of steels and nickel alloys [24–27] have already demonstrated crack growth rates as high as about 10 µm/s in the temperature range 500°C-800°C. It has to be kept in mind that the plastic deformation in the cracking region can strongly accelerate the transport of sulphur to the crack tip. Allart et al. [28] have demonstrated an acceleration by several orders of magnitude of sulphur diffusion during hot deformation of nickel. The high crack growth rate observed here, compared to that estimated from Eq. 2, suggests a strong acceleration of sulphur diffusion to the crack tip, due to plastic deformation. This accelerated diffusion efficiently provides the crack tip with sulphur, which allows fast crack propagation. Similar observations were recently obtained in a study on DDC of an austenitic Fe-Ni alloy, where the accelerated sulphur diffusion to the crack tip was explained by sulphur dragging by moving dislocations [27].

In summary, using model alloys of controlled composition, it was shown that sulphur has a strong deleterious effect on ductility dip cracking of a high chromium nickel alloy. On the other hand, post-mortem analyses using WDS and STEM-EDS showed no GB segregation in cracked specimens, although a control specimen was used to validate the methodology of analysis. The presence of sulphur covering the surfaces created by GB crack propagation suggests a dynamic type of embrittlement, where sulphur feeds the crack tip as it propagates. The surfactant effect of sulphur decreases the surface energy, which facilitates crack opening. The relatively high crack growth rate observed (>~10 µm/s) requires a fast transport of sulphur to the propagating crack tip, which can be achieved by accelerated diffusion of sulphur due to plastic deformation. Considering this mechanism, there is no contradiction between the deleterious effect of sulphur on ductility dip cracking and the absence of sulphur segregation in uncracked GBs of cracked specimens.

Data availability statement

The raw and processed data required to reproduce these findings are available from the corresponding author upon request.

Declaration of Competing Interest

The authors declare that they have no known competing financial interests or personal relationships that could have appeared to influence the work reported in this paper.

Acknowledgment

This research was mainly funded by EDF (Electricité de France) with the support of ANRT (Association Nationale Recherche Technologie). The authors thank Claude Varillon for the preparation of model alloys.

References

[1] G.A. Osinkolu, M. Tacikowski, A. Kobylanski, Mater. Sci. Technol. 1 (1985) 520–525.
[2] G.A. Osinkolu, A. Kobylanski, Scr. Mater. 36 (1997) 1139–1143.
[3] L. Ben Mostefa, G. Saindrenan, M.P. Solignac, J.P. Colin, Acta Metall. Mater. 39 (1991) 3111–3118.
[4] M.T. Perrot-Simonetta, A. Kobylanski, J. Phys. IV France 05 (1995) C7-323-C7-334.
[5] S. Yamaguchi, H. Kobayashi, T. Matsumiya, S. Hayami, Metals Technol. 6 (1979) 170–175.
[6] V. Laporte, A. Mortensen, Int. Mater. Rev. 54 (2009) 94–116.
[7] F.F. Noecker, J.N. Dupont 88 (2009) 62s–77s.
[8] T. Meiners, Z. Peng, B. Gault, C.H. Liebscher, G. Dehm, Acta Mater. 156 (2018) 64–75.
[9] A. Rapetti, F. Christien, F. Tancret, P. Todeschini, S. Hendili, Materials Today Communications (2020) 101163.
[10] A. Rapetti, P. Todeschini, S. Hendili, F. Christien, F. Tancret, in: ASME, 2017, p. V06BT06A022.
[11] C. Fink, J.C. Lippold, A.T. Hope, S. McCracken, in: American Society of Mechanical Engineers Digital Collection, 2017.
[12] A. Rapetti, Fissuration à Chaud Par Chute de Ductilité Dans Les Métaux d'apport Pour Le Soudage d'alliages à Base de Nickel, thesis, Nantes, 2018.
[13] F. Christien, P. Risch, Ultramicroscopy 170 (2016) 107–112.
[14] F. Christien, C. Downing, K.L. Moore, C.R.M. Grovenor, Surf. Interface Anal. 44 (2012) 377–387.
[15] M. Allart, F. Christien, R.L. Gall, P. Nowakowski, C.R.M. Grovenor, Scr. Mater. 68 (2013) 793–796.
[16] A. Larere, M. Guttmann, P. Dumoulin, C. Roques-Carmes, Acta Metall. 30 (1982) 685–693.
[17] P. Nowakowski, F. Christien, M. Allart, Y. Borjon-Piron, R.Le Gall, Surf. Sci. 605 (2011) 848–858.
[18] F. Christien, R.Le Gall, Surf. Sci. 602 (2008) 2463–2472.
[19] A.A. Griffith, G.I. Taylor, Philos. Trans. R. Soc. Lond. Ser. A, Containing Pap. Math. Phys. Character 221 (1921) 163–198.
[20] J.P. Hirth, J.R. Rice, Metall. Trans. A 11 (1980) 1501–1511.
[21] J.R. Rice, J.-S. Wang, Mater. Sci. Eng. 107 (1989) 23–40.
[22] R. Kirchheim, B. Somerday, P. Sofronis, Acta Mater. 99 (2015) 87–98.
[23] A.B. Vladimirov, V.N. Kaigorodov, S.M. Klotsman, I.Sh. Trakhtenberg, Fiz. Met. Metalloved. 39 (1975) 319–323.
[24] D. Bika, J.A. Pfaendtner, M. Menyhard, C.J. Mcmahon, Acta Metall. Mater. 43 (1995) 1895–1908.
[25] C.A. Hippsley, Mater. Sci. Technol. 1 (1985) 475–479.
[26] C.A. Hippsley, H. Rauh, R. Bullough, Acta Metall. 32 (1984) 1381–1394.
[27] F. Christien, Materials 13 (2020) 539.
[28] M. Allart, F. Christien, R.L. Gall, Acta Mater. 61 (2013) 7938–7946.